INVESTIGATIONS OF THE ENERGY RELEASE MECHANISMS OF ALUMINUM-NICKEL REACTIVE MATERIAL SYSTEM

Barrie E. Homan*, Kevin L. McNesby, John Ritter, Joseph Colburn, and Andrew Brant
US Army Research laboratory
Aberdeen Proving Ground, MD, 21005

Ravindra Pandey
Department of Physics
Michigan Technological University
Houghton, MI 49931

ABSTRACT

Reactive materials (RM) are a wide class of energetic materials with unique characteristics that can enable highly lethal munitions along with other applications. Most of the existing information on the behavior of these materials is phenomenological in nature with little evidence as to the initiation and reaction mechanisms at play, making full exploitation of the potential lethality gains difficult. To remedy this situation, a more fundamental understanding of the initiation and reaction processes was pursued by employing combined experimental and theoretical studies. The Ni-Al RM system was chosen as the base for which the morphology, chemistry, and initiation condition effects can be studied. Various metals were mixed or alloyed with the aluminum portion of the RM matrix and were launched by a powder gun into an instrumented chamber to evaluate temperature and pressure.

1. Introduction

The Army has a critical need to fill capability gaps in lethality including incremental nonlethal to lethal effects against personnel and platform, while remaining cognizant of the need for insensitive energetic materials for smart and green munitions. Reactive materials (RMs) are a wide class of energetic materials with unique characteristics that can enable highly lethal munitions for modern tactics like MOUT along with other applications. These materials are more efficient by potentially replacing the parasitic masses associated with any munition as well as efficiently coupling its energy on target. Unlike conventional materials, the insensitivity of these materials increases the power of the munition without simultaneously increasing the vulnerability of the weapon system. At present, there exists only phenomenological evidence as to the initiation and reaction mechanisms that are at play, making full exploitation of the potential lethality gains difficult. To remedy this situation, a combined experimental and theoretical study was implemented with the goal of better understanding the fundamental energy release mechanisms unique to these materials.

The Nickel-Aluminum RM system was chosen as the family of materials for study under this effort for a variety of reasons. Ni-Al is a simple, nominally bi-metallic system that lends itself to modeling and experimental investigations without the complications of organic chemistry that would result from a binder based system. This system's performance has also been extensively cataloged (Ames, 2003, Richards, 2003) and the combination of strength and energy should prove useful to munition designers.

2. PROCEDURE

2.1 Experimental

A matrix of formulations (Table 1) was developed to determine the affects of metal additives on the initiation and combustion properties of the base material. These mixtures of powder ingredients at the desired ratio were isostatically pressed (General Sciences, 2006) under controlled conditions to produce monolithic samples. Being produce this way, the samples tended to have reduced strength that is directly linked to the porosity. The fraction of the theoretical maximum density (TMD) of a typical sample is usually low to mid 90%. Because the cold spray process (Champagne, 2002) for the manufacture of Al-Ni based RM samples has produced samples with densities near 100 % of TMD with improved strength, the effect of the processing technique and mechanical properties was also included in the study. There is anectdotal evidence (Ames, 2003) that this increased strength, while useful for structural components, may also reduce the ability to recover the full energetic potential in lower impact velocity scenarios. Three metal additives, magnesium (Mg), molybdenum (Mo), and copper (Cu) were initially chosen to study the effects of their inclusion on reactivity in the Al-Ni framework. Mg and Mo have shown evidence of enhancing performance (Ames, 2003)

Report Documentation Page

Form Approved
OMB No. 0704-0188

1. REPORT DATE	2. REPORT TYPE	3. DATES COVERED
DEC 2008	**N/A**	**-**

4. TITLE AND SUBTITLE	5a. CONTRACT NUMBER
Investigations Of The Energy Release Mechanisms Of Aluminum-Nickel Reactive Material System	5b. GRANT NUMBER
	5c. PROGRAM ELEMENT NUMBER
6. AUTHOR(S)	5d. PROJECT NUMBER
	5e. TASK NUMBER
	5f. WORK UNIT NUMBER
7. PERFORMING ORGANIZATION NAME(S) AND ADDRESS(ES) **U. S. Army Research Laboratory Aberdeen Proving Ground, MD 21005**	8. PERFORMING ORGANIZATION REPORT NUMBER
9. SPONSORING/MONITORING AGENCY NAME(S) AND ADDRESS(ES)	10. SPONSOR/MONITOR'S ACRONYM(S)
	11. SPONSOR/MONITOR'S REPORT NUMBER(S)

12. DISTRIBUTION/AVAILABILITY STATEMENT
Approved for public release, distribution unlimited

13. SUPPLEMENTARY NOTES
See also ADM002187. Proceedings of the Army Science Conference (26th) Held in Orlando, Florida on 1-4 December 2008, The original document contains color images.

14. ABSTRACT

15. SUBJECT TERMS

16. SECURITY CLASSIFICATION OF:			17. LIMITATION OF ABSTRACT	18. NUMBER OF PAGES	19a. NAME OF RESPONSIBLE PERSON
a. REPORT	b. ABSTRACT	c. THIS PAGE			
unclassified	**unclassified**	**unclassified**	**UU**	**8**	

while Cu was considered because of its large effects on the melting point of Al.

Table 1. Tested formulations

Description	Formulation (% by weight)	Density (g/cc)	Mass (g)
Cold spray	Al/Ni 30/70	5.2	3.8
Pressed	Al/Ni 31.5/68.5	4.6	7.7
Molybdenum	Al/Mo/Ni 30.3/2.2/67.5	4.9	7.9
Magnesium	Al/Mg/Ni 28.6/2.4/69.0	4.7	7.6
Copper	Al/Cu/Ni 24.2/11.7/64.1	5.2	8.6

A new experimental facility has been designed and implemented that improves on similar facilities in the Navy and Air Force. The centerpiece of the new facility is the reaction chamber, dubbed the 'Green Pig' in deference to the aptly named 'Blue Pig" operated by the Navy. The Blue Pig consists of a section of industrial pipe with appropriate flanges to seal the ends. (Ames, 2003) The Green Pig (Figure 1), has a suite of diagnostic instruments that has been developed and implemented to determine the mechanical state of the projectile (amount of disintegration), and the timing and quantity of the energy released. These tools include pressure, pyrometry, emission spectroscopy, heat flux, and high-speed, high-brightness imaging. However, only the imaging and pyrometry data is discussed in this paper. As the particulates, especially reacting particulates, may have a different temperature than that of the surrounding gas, a two-wavelength, high-speed, spatial pyrometry technique has been developed. If the wavelengths chosen are in a region of the spectrum not dominated by the atomic or molecular gas phase emission, the pyrometry technique will be unaffected by the local gas temperature.

Figure 1. Reactive Material Research Facility's Green Pig.

2.2 Modeling

Using first principles calculations, we have studied one of the prevalent mechanisms of energy release typified by the energetic alloying behavior of the Ni-Al RM system. The proposed system consists of Ni particles of controlled sizes embedded into an Al matrix. We have characterized the chemical and mechanical response of nanostructured reactive materials using a finite quantum cluster model that captures microscopic processes governing both the initiation and reaction processes in these materials. Previously, the structural stability of Ni_mAl_n clusters consisting of 12 to 55 atoms was examined in the framework of an atomistic model (Rexer, 2002; Parks, 2002; Jellinek, 1996; Krissinel 1997) which employed interatomic potentials derived from embedded atom method. It was concluded that a thirteen-atom Ni_mAl_n cluster prefers an icosahedral derived arrangement of atoms in its ground state configuration.

The system studied consisted of Ni_xAl_{13-x} clusters with x=0-13 in an icosahedral configuration. Specifically,

(i) We have calculated the compositional stability of Ni_xAl_{13-x} clusters performing geometry optimization of several cluster configurations varying x. Since the energy surface is expected to have multiple local minima, we have performed finite temperature simulation as a prelude to final optimization of atomic positions of a given cluster.

(ii) We have further calculated the melting point of Ni_xAl_{13-x} clusters using the first principles thermodynamic Car-Parrinello method knowing that understanding of mechanism of melting will shed the light on the initiation mechanism of nanostructured Ni/Al reactive materials since initiation temperature of ignition is directly related to melting temp.

3. RESULTS

3.1 Experimental

The sabot/RM projectiles were launched from a 30 mm smooth bore powder gun at an average velocity of 1615 +- 39 m/s. The sabot was a two piece designed that is stripped from the flight path. The velocity was measured by three break screens with the last screen mounted to the front of the pig and acting as the time zero fiduciary mark. The main chamber is separated from the pre-chamber by an impact plate that can be varied in thickness as well as material. For the results discussed

here, the impact plate parameters, mild steel of 1/16" (0.158 cm) thick, were kept constant. Inside the chamber a second plate of RHA steel 2" thick acted as an anvil. In figure 2, a series of high speed images from a typical experiment is shown. The high speed camera frequency was 20,000 frames per second (fps) or 50 us between frames. A break screen, used as the time fiduciary, is just to the left of the pre-chamber wall seen most clearly in the 210 us image. The projectile punches out a small section of the paper as it passes through and the heat generated from this interaction is enough to ignite the paper as seen in the 10 us image. At 210 us, the projectile material has just penetrated the impact plate. A fair amount of emission from this impact can be seen on the pre-chamber side. At 710 us, there is still reactivity seen in the pre-chamber. Finally, at 760 us the cloud of RM begins to impact the anvil. Using the known distances and times, the fragment cloud is traveling at approximately 1,340 m/s or at a 17% reduction in velocity from pre-impact. Although there is some amount of RM reacting from the first impact at 210 us, it is clear that the majority of the energy stored in the sample is being released upon interaction with the anvil.

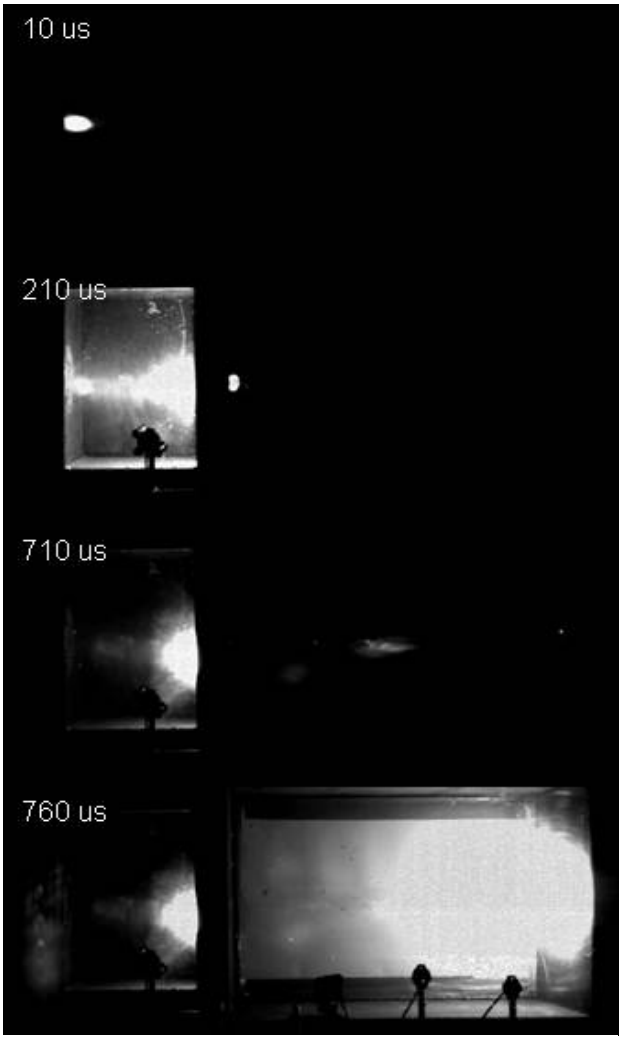

Figure 2. High speed imaging.

Due to the lack of the camera dynamic range exacerbated by the bright emission inherent in the reaction of energetic materials, it is difficult to capture the non emitting elements without complete saturation of bright regions resulting from reaction events. A second instrumental technique, high brightness imaging (HBI), was incorporated to probe those regions that are not visible with other methods during emission. In this technique (McNesby, 2005), a high power, short pulse duration (20 ns) laser with wavelength of 510 nm is synchronized to a high speed camera incorporating an appropriate band pass filter. The band pass filter, centered on the 510nm wavelength with a widow of +- 5nm minimizes the emission from the event by admitting only a small section of the continuous spectrum. Because the camera is sensitive only to the wavelength of the light, the exposure setting can be made very short (1 or 2 us) and still see the entire duration of the laser light while reducing the amount of the relatively long time frame light from the reaction. Three images from the HBI movie of the Al-Mo-Ni sample are shown in Figure 3. The field of view (FOV) of these images encompasses approximately half of the main chamber with the anvil at the right edge of the frames. As the RM particle cloud enters the FOV from the left, a typical mushroom shape of debris is clearly discernable

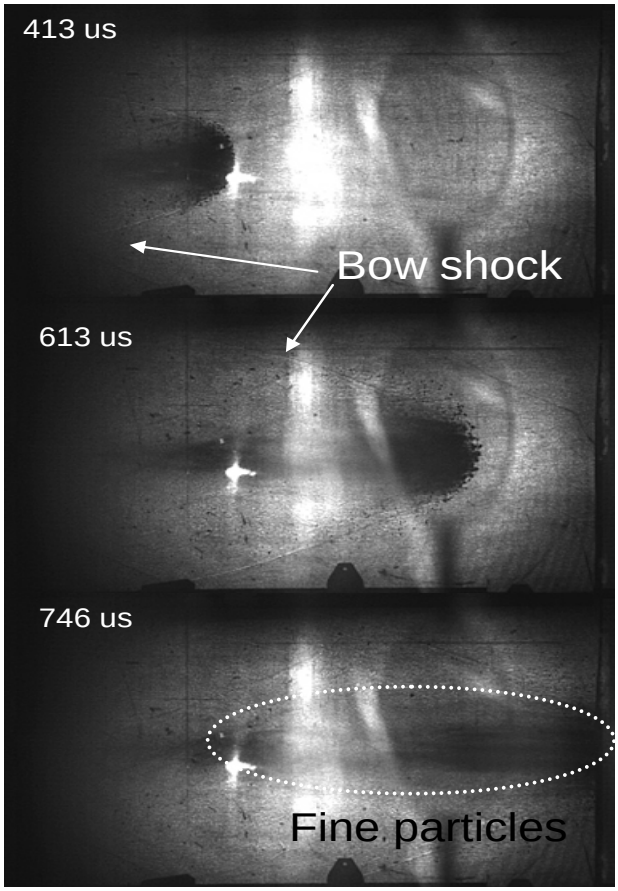

Figure 3. High Brightness imaging.

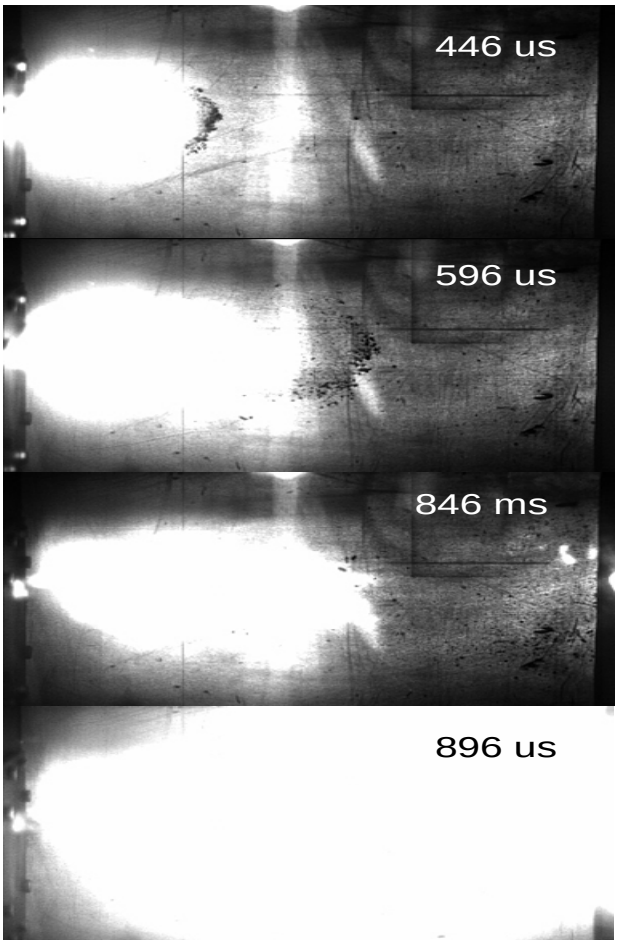

Figure 4. High brightness imaging without laser filter.

with accompanying bow shock being imaged. The particles are being sorted by mass due to aerodynamic drag with the heavier particles retaining the highest velocity. At 613 us (microseconds) the heaviest particles, with the greatest momentum, are overtaking the shock. Finally, at 746 us, the initial particles have impacted the anvil but a cloud of fine particles remains in the chamber. Similar behavior is seen in Figure 4. This figure is also from the HB technique but the band pass filter was not used. Although clear saturation is evident, some of the non emitting particles are also evident. The Ni-Al sample depicted here was produce by the cold spray process. Early on (446 us) the heaviest particles are seen emerging from the fireball produced from the initial impact. As the event unfolds, these particles begin to separate from that fireball. At 846 us, just as the first of the particles are impacting the anvil, there is a cloud of fine particle stretching back to into the fireball. 50 us later, at 896 us, the region containing the fine particle is rigorously reacting as evident from the emission signature in a similar fashion that is reminiscent of a fuel air type explosion.

By using an imaging spectrometer coupled to fiber optics placed at strategic regions along the trajectory inside the pig, information as to the gas phase chemistry can be obtained (McNesby, 2005b). To obtain temporal information, the spectrometer used a high speed camera (Vision Research Phantom 7.3) running at 11,000 fps as its detector. A snapshot at t=900 us (microseconds) of the four formulations tested here is shown in Figure 5. The different formulations are arranged in rows while the different regions are arranged in columns. The first region at left in the figure is due to reactions inside the pre-chamber. Second from the left captures the chemistry occurring in the region directly downstream of the impact plate. Third from the left collects light from the central portion of the main chamber between the impact plate and anvil. Finally, the rightmost column represents the region of impact near the anvil. The samples follow that listed in table 1 with the top being the pressed powder Al-Ni base and the bottom containing Cu as a modifier. The spectral region represented here is 450-550 nm selected with the expectation of capturing species like AlO that have a band

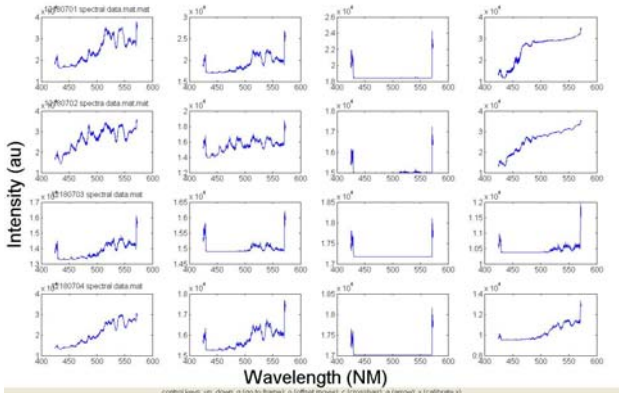

Figure 5. Emission spectroscopy data.

head at 484.2 nm. This data is preliminary at this point and further analysis is underway.

Rounding out the optical diagnostics is a two-color, high speed imaging pyrometer developed in house. The heart of the system is two high speed cameras (Vision Research Phantom 5.1) operating a 10,000 fps. Each camera sees the same view through a set of optics that includes a beam splitter. In front of each camera is a narrow band pass filter (700 or 900 nm and a band with of 10nm). The movies from each camera are calibrated using a black body source at 1000 C. Using Planck's blackbody relationship (McNesby, 2004), the temperature map as a function of time can be calculated from the ratio of the intensities recorded from the two cameras. In figure 6, the first temperature map captured after anvil impact is compared for the four classes of samples. On the left in the figure is the spatial temperature map data while on the right is a corresponding histogram of temperatures. The

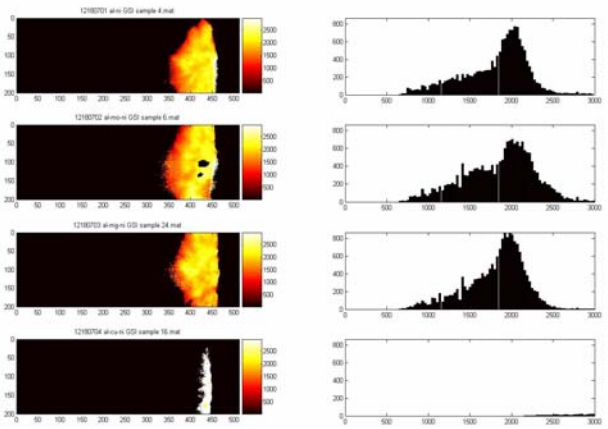

Figure 6. Pyrometer imaging at t=800 us.

black hole seen in the Al-Mo-Ni map is due to detector saturation for which the temperature cannot be calculated. The histogram provides a good indication of the predominant temperatures seen. The base material along with the Mg modified sample produced similar maximum temperatures of near 2500 K. The Mo modified material increased the initial reaction temperature by about 200 K. The greatest difference occurred by adding Cu to the base material. The initial temperatures increased over 500 K to 3000K. Later on in the event, seen in figure 7, the base, Mo, and Mg formulations are similar in their temperature profile. The overall thermal field has cooled from the initial conditions and a bi-modal temperature distribution is apparent in both the maps and histogram. The cooler region is on the leading edge of the fireball (on the left) as would be expected for an expansion waves. However, in the case of the Cu based formulation, the maximum temperature remains high with the highest temperatures seen at the front of the fireball indicating possible reactions still occurring in this region.

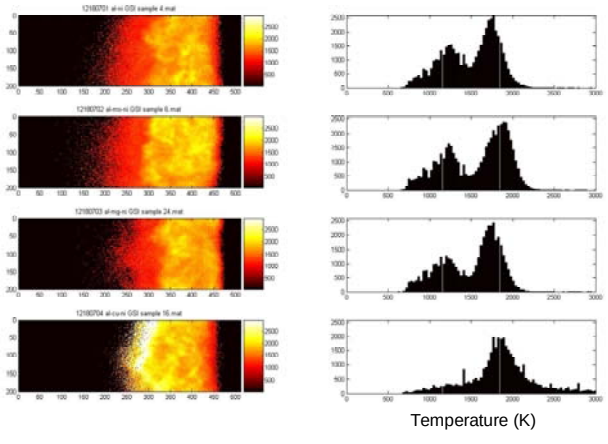

Figure 7. Pyrometer imaging at t=1400 us **.**

3.2 Modeling

The electronic structure calculations were performed in the framework of density functional theory using ultrasoft pseudopotentials. The exchange-correlation functionals considered were the local spin density approximation of Vosko, Wilk, and Nusair (Vosko, 1980) (VWN) and generalized gradient approximation (GGA) given by Perdew and Wang (Perdew, 1992) (PW-91) as implemented in the program package VASP (Vienna, 1999). The computational parameters were taken from our previous studies (Deshpande, 2005) in which atoms in a given cluster were positioned in a cubic supercell with an edge of 20 A. The cutoff energy for the plane wave basis was set to 241.6 eV and reciprocal space integrations were performed at the Γ point.

We began with *first principles* calculations to study the phase stability of NiAl system in both solid state and nanoscale regime. The NiAl alloy system is found to occur in several phases, including Ni_3Al, Ni_5Al_3, NiAl, Ni_2Al_3, $NiAl_2$ and $NiAl_3$. The calculations showed the cohesive energy of these phases to be stable with the lowest energy being associated with the stoichiometric NiAl alloy. Likewise, stability of the stoichiometric composition is predicted in the nanoclusters regime confirming the fact that similar nature of chemical bonding exists in both solid state and nanoscale regime. The calculated results therefore show the accuracy and reliability of the modeling elements, e.g. functional form, basis sets and pseudopotentials employed in this study**.** The initial choices of the configuration for the geometry optimization are based on the icosahedra-derived configurations, both Ni- and Al-centered. Note that several studies (Rexer, 2002; Parks, 2002; Jellinek, 1996; Krissinel 1997) have found the preferred configuration for thirteen-atom $Ni_{12}Al$ or $NiAl_{12}$ cluster to be a Ni-centered icosahedra-derived configuration (e.g. Figure 8).

As a rule, atomic arrangements with which we dealt have a complicated energetic surface rich with local

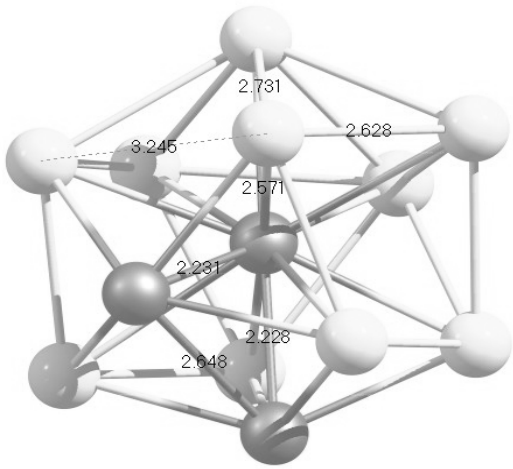

Figure 8: The icosahedral configuration of Ni_xAl_{13-x} cluster.

minima. Therefore, starting from such icosahedral-like configurations, we used the simulated annealing strategy to perform the geometry optimization calculations. In the simulated annealing step, the initial cluster configuration was heated to 800-900 K, thus allowing it to sample other regions of configuration space. This was followed by a slow cooling to obtain the equilibrium cluster configuration. The stability of the equilibrium ground state configuration and some of the low-lying isomeric configurations of a given cluster were further checked by performing calculations in different spin configurations as well. As an additional test, a symmetry-constrained geometry optimization keeping the icosahedral symmetry was also performed on these clusters. The cluster configurations were considered to be converged when the force on each ion was less than 0.01 eV/A with a convergence in the total energy of about 10^{-6} eV. Optimized configurations obtained from *first principles* calculations providing details of configurations associated with the ground and low-lying metastable states of Ni_xAl_{13-x} clusters. Figure 9 shows that the introduction of a Ni atom in a Al_{13} cluster yields a higher (4%) binding energy. Overall, the Ni-excess clusters tend to have a higher binding energy than the Al-excess clusters for the thirteen-atom Ni_xAl_{13-x} series considered. It is consistent with the fact that the ordered Ni_3Al phase has a higher bulk cohesive energy (4.7 eV) than either bulk nickel (4.4 eV) or aluminium (3.39 eV). Note that for Ni_2, Ni-Al and Al_2 diatomic molecules, the respective binding energy per atom is 1.31, 1.35, 0.86 eV/atom, and the respective bond length is 2.09 A, 2.22 A and 2.51 A. Therefore, the Al-Al bonds are clearly not preferred with respect to either Ni-Al or Ni-Ni bonds.

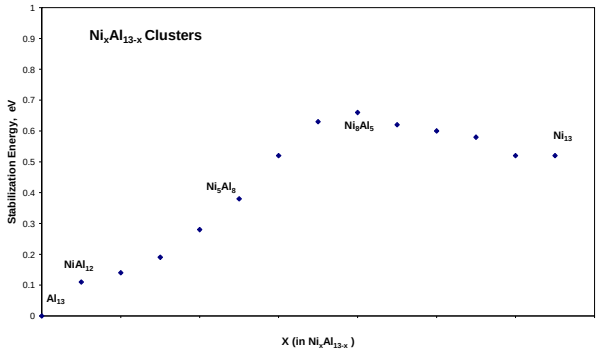

Figure 9: Gain in stabilization energy (relative to Al_{13}) of Ni_xAl_{13-x} clusters. Substitution of a Ni atom in $NiAl_{12}$ leads to about 4% higher strength in Al_{13}.

A quite simple explanation of the enhanced stability of Ni-Al clusters can be obtained from hybridization of the cluster electronic orbitals. When we replace an Al atom by a Ni atom in Al_{13} cluster, the resulting electronic configuration of $NiAl_{12}$ will be different from that for Al_{13}. The number of states available varies: the diffuse *s* and *p* states associated with Al will undergo a strong hybridization with their environment, thus lowering their energy. The increase in the cluster stability with the increase in the Ni concentration can then be attributed to the greater degree of hybridization that forces the pairing of the electrons in the mixed orbitals of Ni and Al. A similar previous theoretical study (Payne, 1992) of B-Ni alloy, our group found that Ni atoms appeared to significantly influence the stability and electronic properties of the boron clusters.

For the melting of Ni_xAl_{13-x} Clusters**,** we have employed Bohn-Oppenheimer molecular dynamics (Payne, 1992) using projector augmented wave (PAW) pseudopotentials (Kresse, 1999; Blöchl, 1994) within the local density approximation as implemented in the VASP package. A cubic supercell of length 20 Ã was used for the total-energy convergence. The energy cutoffs or the plane wave basis set and the augmentation charges were set to 270 eV and 545 eV, respectively. The icosahedral (optimized) structure considered were Al_{13}, Ni substituting Al at the center or the surface of the Al_{13} icosohedron, labeled as Al_{12}Ni_center and Al12Ni_surface, respectively. To examine the finite temperature behavior of clusters, molecular dynamics simulations have been carried out at several temperatures for these clusters within the range of 350 K to 950 K. The simulation time for each temperature is 30 ps. The resulting trajectories have been used to calculate standard thermodynamic indicators as well as the ionic specific heat via multiple histogram technique.

The melting temperature of a given cluster can be identified with the peak in the heat capacity curve. Figure 10 shows the specific heat capacity curves for Al_{13}, Al_{12}Ni_center and Al_{12}Ni_surface clusters calculated by sampling the phase space at various constant temperatures. The multiple histogram method was used to compute the heat capacity ensuring that an adequate overlap in the potential energy distribution was obtained in the range of temperatures considered. The method extracts the classical ionic density of states (C(E)) of the cluster, or equivalently the classical ionic entropy $S(E) = k_B \ln C(E)$, from the simulation data. Knowing S(E), one can evaluate thermodynamic averages in a variety of ensembles. More technical details concerning the extraction of thermodynamics averages, indicators and computation of the specific-heat curve can be found in reference Vichare, 2006.

The (high temperature) broad peak for Al_{13} is around 800 K whereas the peak is at about 1000K for Al_{12}Ni_center. For the Al_{12}Ni_surface cluster, a narrow peak at about 600K appears in Fig. 7. The addition of Ni at

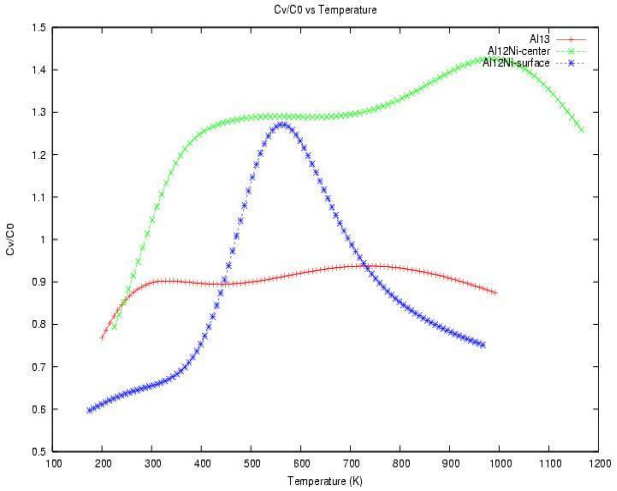

Figure 10: Normalized specific heat for Al_{13}, $Al_{12}Ni$_center and $Al_{12}Ni$_surface clusters. The melting temperature can be identified with the peak in the heat capacity curve.

the surface of Al_{13} cluster therefore appears to lower the cluster melting temperature in contrast to the prediction of a higher cluster melting temperature when Ni is embedded in the Al_{13} cluster.

4. CONCLUSIONS:

A variety of formulations based on the Al-Ni family of reactive materials has been investigated. A suite of diagnostic techniques has been applied to investigate the initiation and combustion behavior of these materials. The sequence of events starts with the pulverization of the RM by penetration through the impact plate. Although some of the chemical energy is released in this interaction, the majority is preserved as the debris field continues into the chamber. As the material travels, the particles are sorted by size due to aerodynamic forces. As the heaviest particles hit the anvil they initiate a reaction that generates a reaction wave passing through the finer particles throughout the chamber. Addition of different metals to the formulation affects the combustion process in different ways. The addition of Mg at this concentration had little effect. The Mo modified material showed slightly higher temperatures early on with that difference decreasing further into the event. The addition of Cu, however, showed a marked increase in initial temperature as well as evidence of continued reaction further into the chamber.

First principles calculations based on density functional theory were performed to examine the compositional stability of NiAl system. In both solid state and nanoscale regime, the stoichiometric composition is found to be stable suggesting that the structural properties exhibited by the NiAl nanoclusters will be similar to those exhibited by the NiAl alloy. This is what we expected, thus showing the accuracy and reliability of the modeling elements employed. An icosahedral Ni_xAl_{13-x} cluster configuration was chosen to simulate Ni particles embedded into an Al matrix. The sequential addition of Ni in Al_{13} is found to increase the cluster binding energy as we go from Al_{13} to Ni_xAl_{13-x} to Ni_{13}. For example, addition of a Ni atom in a Al_{13} cluster yields about 4% gain in energy due to strengthening of the bonds accompanied with a small, but noticeable contraction in the volume of the cluster. The optimized configurations of $NiAl_{12}$ clusters were used to perform *first principles* thermodynamic simulations to calculate melting point of Al_{13}, $Al_{12}Ni$(center) and $Al_{12}Ni$(surface) clusters. The results predict the increase in the melting point upon substitution of nickel at the center of the icosahedral Al_{13} cluster whereas substitution of Ni at the surface lowers the melting point. The calculated results, for the first time, have *'quantified'* the effect of addition of Ni particles in the Al matrix in terms of the bond length, bond energy and melting point in the nanoscale cluster regime.

5. ACKNOWLEDGMENTS

The authors thank Shashi P. Karna and Govind Mallick for many helpful discussions. We would also like to thank Joseph Colburn and Andrew Brant for the operation of the powder gun used to launch the samples. The authors also thank General Science Inc. for producing the samples.

6. REFERENCES

Ames, R., 2003: .Naval Surface Warfare Center Program Summary, XB-NSWCDD/VA.

Blöchl, P. E., 1994: Phys. Rev. B 50, 17953.

Champagne, V.K., "The Cold Spray Deposition Process: Fundamentals and Applications", CRC Press.

Deshpande, M.D., Kanhere, D. G., and Pandey, R., 2005: Phys. Rev. A, 71, 063202.

General Sciences Inc, 2006: "Final Report on Reactive Materials as Lethality Enhancers".

Kresse, G., and Joubert, D., 1999: Phys. Rev. B 59, 1758.

Jellinek, J., and Krissinel, E. B., 1996: Chem. Phys. Lett. 258, 283.

Krissinel, E. B., and Jellinek, J. 1997: Int. J. Quantum Chem. 62, 185.

McNesby, K.L., and Homan, B.E., 2005a: ARL Technical Report, ARL-TR-3483.

McNesby, K.L., Homan, B.E., and R.E. Lotterro 2005b, ARL Technical Report, ARL-TR-3411.

McNesby, K.L., Homan, B.E., Piehler, T.N., and Lottero, R.E. 2004: ARL Technical Report, ARL-TR-3318.

Parks, E. K., Rexer, E. F., and Riley, S. J., 2002: J. Chem. Phys. 117, 95.

Payne, M. C., Teter, M. P., Allan, D. C., Arias, T. A., and Joannopoulos, J. D.,1992: Rev. Mod. Phys. 64, 1045.

Perdew J. P. and Wang, Y., 1992: J. Chem. Phys. 45, 13244.

Rexer, E. F., Jellinek, J., Krissinel, E. B., Parks, E. K., and Riley, S. J., 2002: J. Chem. Phys. 117, 82.

Richards, D.W., Kramer, M.P., and Wilson, W.H., 2003: Air Force Research Laboratory Technical Report, AFRL-MN-EG-TR-2004-7013.

Vichare, A., Kanhere, D. G., and Blundell, S. A., 2006: Phys. Rev. B 64, 045408 (2001); S. Krishnamurty, K. Joshi, D. , G. Kanhere, and S. A. Blundell, ibid. 73, 045419.

Vienna, 1999: Vienna *Ab initio* Simulation Package(VASP), Technishe universitaöt, Wien.

Vosko, S. H., Wilk, K., and Nusair, N., 1980: Can. J. Phys. 58, 1200.